APL Materials

RESEARCH ARTICLE | JULY 07 2023

Excitation wavelength dependent triple-mode photoluminescence of copper-based halides for advanced anti-counterfeiting

Chengjun Liu ; Yuyi Zhang; Manman Luo ; Lixi Wang ; Xingyu Liu; Jiangyong Pan ; Zihan Zhao; Fan Fang; Lei Mao ; Yuling Huang ; Bingqi Wang; Congyuan Lin ; Wei Lei ; Qing Li; Zhiwei Zhao; Jun Wu; Zhuoya Zhu; Mehmet Ertugrul ; Xiaobing Zhang ; Jing Chen ; Dewei Zhao

Check for updates

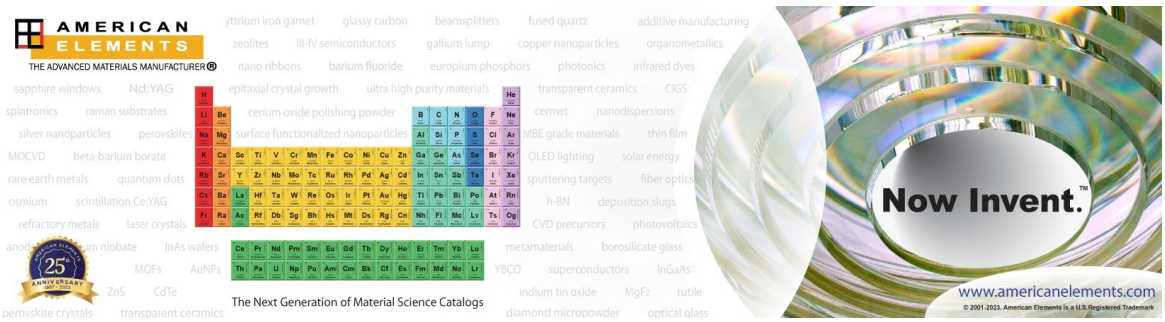
APL Mater. 11, 071109 (2023)
https://doi.org/10.1063/5.0152479

CrossMark

View Online

Export Citation

24 December 2023 15:22:00



AIP Publishing

Excitation wavelength dependent triple-mode photoluminescence of copper-based halides for advanced anti-counterfeiting

Cite as: APL Mater. 11, 071109 (2023); doi: 10.1063/5.0152479
Submitted: 30 March 2023 • Accepted: 5 June 2023 •
Published Online: 7 July 2023

View Online Export Citation CrossMark

Chengjun Liu,[1] Yuyi Zhang,[1] Manman Luo,[1] Lixi Wang,[2] Xingyu Liu,[1] Jiangyong Pan,[2,a)] Zihan Zhao,[1] Fan Fang,[1] Lei Mao,[2] Yuling Huang,[2] Bingqi Wang,[2] Congyuan Lin,[2] Wei Lei,[1] Qing Li,[1] Zhiwei Zhao,[1] Jun Wu,[1] Zhuoya Zhu,[1] Mehmet Ertugrul,[3,4,5] Xiaobing Zhang,[1,a)] Jing Chen,[1,a)] and Dewei Zhao[6,a)]

AFFILIATIONS

[1] Joint International Research Laboratory of Information Display and Visualization, School of Electronic Science and Engineering, Southeast University, Nanjing, China
[2] School of Electronics and Information Engineering, Nanjing University of Information Science and Technology, Nanjing, China
[3] Department of Electrical and Electronics Engineering, Ataturk University, Erzurum 25240, Türkiye
[4] Department of Electrical and Electronics Engineering, Universiti Putra Malaysia, UPM Serdang, Selangor 43400, Malaysia
[5] Department of Electric and Electronics Engineering, Kyrgyz Turkish Manas University, 56 Chyngyz Aitmatov Avenue, Bishkek, Kyrgyz Republic
[6] College of Materials Science and Engineering & Engineering Research Center of Alternative Energy Materials & Devices, Ministry of Education, Sichuan University, Chengdu 610065, China

[a)] **Authors to whom correspondence should be addressed:** pjy@nuist.edu.cn; bell@seu.edu.cn; chenjing@seu.edu.cn; and dewei.zhao@scu.edu.cn

ABSTRACT

New fluorescent materials with a low cost, hypotoxicity, and concealment are desired for the application of anti-counterfeiting. Herein, we report a $CsCu_2I_3$@$Cs_3Cu_2I_5$ composite with a triple-mode photoluminescence (PL) feature by simply adjusting the excitation wavelengths, which are ascribed to the multiple excited states of different phases in the $CsCu_2I_3$@$Cs_3Cu_2I_5$ composite. The broadband emission and high quantum yield (~51%) of the composite originate from the structure-oriented self-trapped excitons effect of $Cs_3Cu_2I_5$ and $CsCu_2I_3$ phases. Moreover, the incorporation of polyethylene oxide (PEO) into this composite improves the stability of $CsCu_2I_3$@$Cs_3Cu_2I_5$@PEO against harsh environments. The $CsCu_2I_3$@$Cs_3Cu_2I_5$@PEO composite has a slight decay of ~5% of its initial PL intensity and only a 3.5% shift of the corresponding color coordinate after 30 days of storage. More importantly, its initial PL intensity shows only 10.3% decay under ultraviolet exposure for 200 h. Our work provides a promising approach to design materials for advanced anti-counterfeiting applications.

© 2023 Author(s). All article content, except where otherwise noted, is licensed under a Creative Commons Attribution (CC BY) license (http://creativecommons.org/licenses/by/4.0/). https://doi.org/10.1063/5.0152479

INTRODUCTION

Counterfeiting phenomena, such as fake banknotes, security, documents, and certificates, are a growing global issue that has caused six trillion USD in economic loss.[1–5] Various strategies have been developed for anti-counterfeiting applications to avoid financial losses, including watermarks, holograms, luminescence, barcodes, and two-dimensional codes.[6,7] Among these anti-counterfeiting strategies, the luminescent anti-counterfeiting technology based on fluorescent anti-counterfeiting materials exhibits its advantages of easy operation, simple design, and mass production.[8] However, facing rampant counterfeiting phenomena, simple fluorescent anti-counterfeiting materials cannot meet the increasing demand for anti-counterfeiting anymore.[8–11]

Luminescent anti-counterfeiting technology can be classified into three levels from basic to advanced one: single-level anti-counterfeiting, double-level anti-counterfeiting, and multi-level anti-counterfeiting. Among those, the multilevel anti-counterfeiting

24 December 2023 15:22:00

© Author(s) 2023

should exhibit at least three colors by external stimuli, which can effectively prevent the information from being decoded and greatly improve the information security.[8,12–18] Although luminescent anti-counterfeiting applications have been widely reported, advanced anti-counterfeiting materials with triple-mode luminescence are rarely reported.[8,12,16–21] Lin *et al.*[19] prepared anti-counterfeiting labels by adding the mixture of Tm:$KYbF_7$@glass powders and $CsPbBr_xI_{3-x}$ perovskite nanocrystals@glass powders into a commercial blank white screen-printing ink to form the anti-counterfeiting ink, labeling the blue and the red under the excitation of near-infrared (NIR) and ultraviolet (UV) light, respectively. Moreover, the anti-counterfeiting ink exhibited the mixed blue and red emissions when excited by superimposed NIR light and UV light. Moreover, Wang *et al.*[16] constructed high-performance $CsPbBr_3$@Cs_4PbBr_6/SiO_2 composites via the modified reprecipitation method, which simultaneously exhibit triple-mode emission. Wang *et al.*[18] reported $CaTiO_3:Pr^{3+},Er^{3+}$ that simultaneously displays afterglow, up-conversion luminescence, and excitation wavelength-responsive color evolution photoluminescence (PL) emission.

Limitations still exist in these strategies that hinder practical applications, including the toxicity of lead, slow switching speeds between different modes, complex synthesis methods, specific working conditions (combination of pressure, temperature, and humidity), and the instability caused by the mixture of different fluorescent materials. Therefore, it is highly urgent to develop effective and facile materials with multimodal luminescent features capable of combating sophisticated counterfeiters.

In this work, we report the copper-based halides $CsCu_2I_3$@$Cs_3Cu_2I_5$ featuring with triple-mode PL properties located at 441 or 580 nm, or a mixture of them for advanced anti-counterfeiting applications. Our theoretical calculation and experimental characterization results indicate that the triple-mode PL emission originates from the structure-oriented self-trapped excitons (STEs) effect of $Cs_3Cu_2I_5$ and $CsCu_2I_3$ phases. Moreover, the incorporation of polyethylene oxide (PEO) can not only make the $CsCu_2I_3$@$Cs_3Cu_2I_5$ composite resist high temperatures, oxygen, and moisture but also improve the PL quantum yield (PLQY). Our work offers a promising and robust way to prepare an effective and stable anti-counterfeiting ink for the protection of high-value commodities, government documents, and banknotes in the future.

RESULTS AND DISCUSSION

The x-ray diffraction (XRD) patterns of the $CsCu_2I_3$@$Cs_3Cu_2I_5$ composite show that the as-prepared film is a composite of zero-dimensional $Cs_3Cu_2I_5$ and one-dimensional $CsCu_2I_3$. As shown in Fig. 1(a), the crystal structures of $CsCu_2I_3$ and $Cs_3Cu_2I_5$ belong to the orthorhombic crystal system with the space groups of Cmcm and Pnma, respectively.[22–25] The peaks at 10.5°, 21.5°, and 43.6° correspond to the $CsCu_2I_3$ phase, while the peaks at 13.1°, 23.7°, 26°, and 30.4° are associated with the $Cs_3Cu_2I_5$ phase, which indicate the composite film is composed of $CsCu_2I_3$ and $Cs_3Cu_2I_5$ phases.[26] The SEM and energy dispersive spectroscopy (EDS) results of $CsCu_2I_3$@$Cs_3Cu_2I_5$ show that the elements of Cs, Cu, and I are distributed uniformly [Figs. 1(b)–1(e)], revealing the uniform composition of the film. Furthermore, the quantitative EDS analysis indicates that the atomic ratio (%) of Cs, Cu, and I is 1.00:1.09:2.19 (Fig. S1), which coincides with the stoichiometry of the $CsCu_2I_3$@$Cs_3Cu_2I_5$ composite.

We investigated the optical properties of the composite film by measuring the steady-state PL spectra as shown in Fig. 2. The

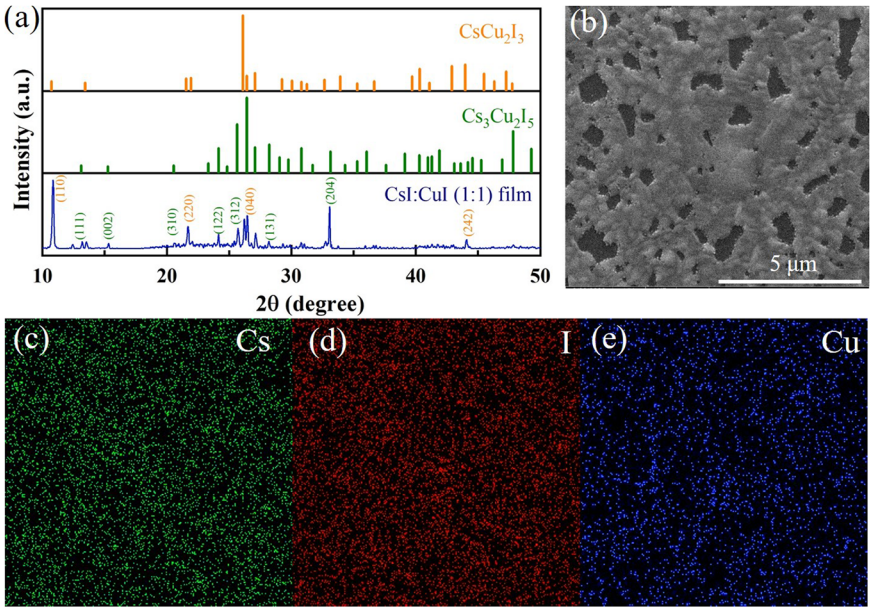


FIG. 1. (a) XRD patterns of $CsCu_2I_3$, $Cs_3Cu_2I_5$, and $CsCu_2I_3$@$Cs_3Cu_2I_5$; (b) SEM image of $CsCu_2I_3$@$Cs_3Cu_2I_5$ and EDS mappings of $CsCu_2I_3$@$Cs_3Cu_2I_5$; (c) Cs, (d) I, and (e) Cu.

24 December 2023 15:22:00

© Author(s) 2023

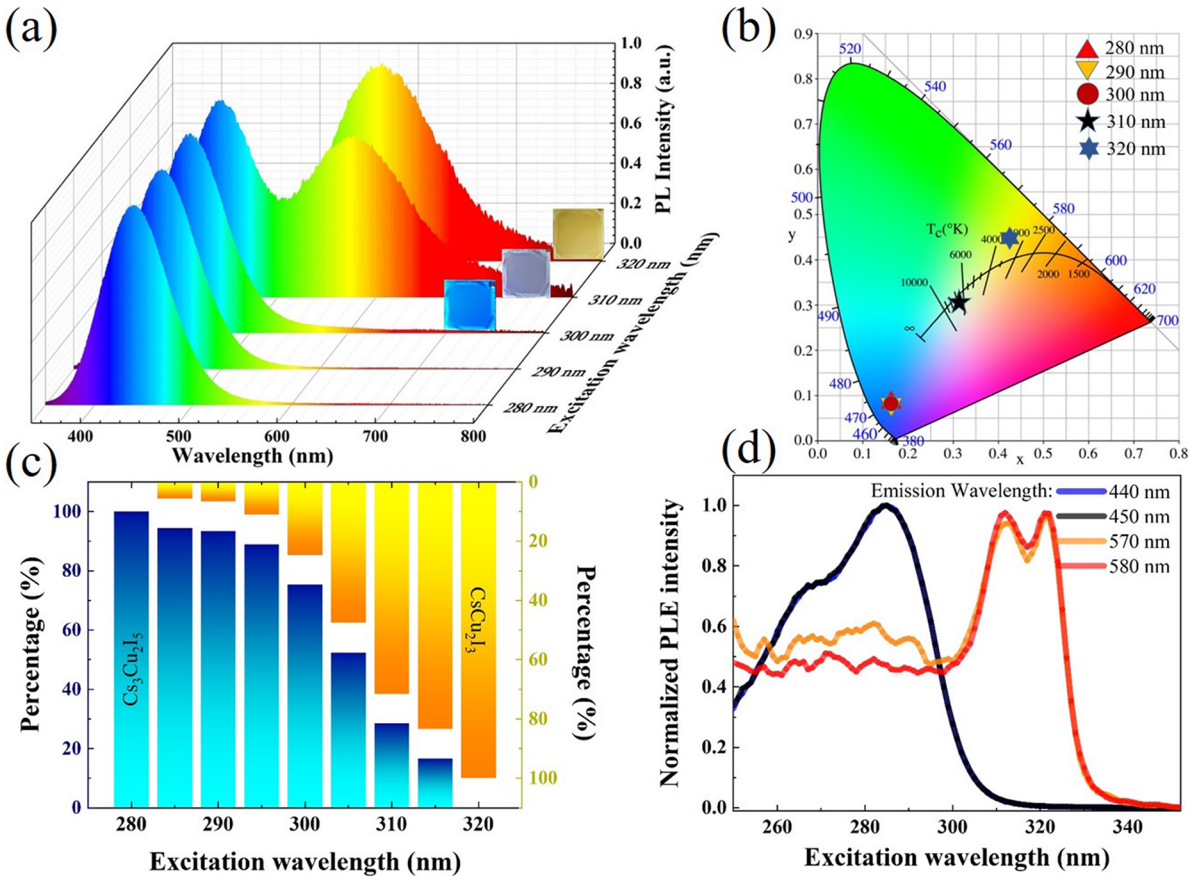


FIG. 2. (a) PL spectra under excitation by different wavelengths. The insets display the corresponding photographs of the film and (b) Commission Internationale de L'Eclairage (CIE) of the $CsCu_2I_3$@$Cs_3Cu_2I_5$ film. (c) Comparison of the proportion of PL intensity of $CsCu_2I_3$ and $Cs_3Cu_2I_5$ emissions under different excitation wavelengths. (d) PLE spectra of the $CsCu_2I_3$@$Cs_3Cu_2I_5$ film under different emission wavelengths.

composite film exhibits a bright blue emission located at 441 nm with a large full-width at half maximum (FWHM) of ~80 nm under 300 nm or shorter wavelength excitation, which originates from the $Cs_3Cu_2I_5$ phase.[27] With the excitation wavelength increasing from 300 to 310 nm, the blue emission gradually evolves to the white emission. Two distinct peaks at 441 and 580 nm can be observed from the PL spectra, which are assigned to the emission from the excited-state structural reorganization and the self-trapped exciton of the $Cs_3Cu_2I_5$ and $CsCu_2I_3$ phases, respectively.[22,28–33] It is noted that the emission peaks for $Cs_3Cu_2I_5$ and $CsCu_2I_3$ is different from those reported by Ma *et al.*[28] We attribute this difference to the different fabrication parameters, which results in the obtained copper-based halides film deviating slightly from strict stoichiometric ratios. With the excitation wavelength further increasing to 320 nm, the white emission of the composite film eventually turns to a yellow one with the peak located at 580 nm and an enlarged FWHM of ~125 nm [Fig. 2(a)]. Accordingly, the Commission Internationale de L'Eclairage (CIE) color coordinates shift from blue region (0.15, 0.07) to white region (0.32, 0.30), and eventually to yellow region (0.43, 0.45) with the increase of excitation wavelength [Fig. 2(b)]. Figure 2(c) shows the relative PL intensity of $Cs_3Cu_2I_5$ and $CsCu_2I_3$ phases under different excitation wavelengths.

In order to explore the origins of the excitation-wavelength-dependent PL, the PL excitation (PLE) spectra of the $CsCu_2I_3$@$Cs_3Cu_2I_5$ composite film measured at different emission wavelengths are shown in Fig. 2(d). For the excitation spectra monitored at 450 nm corresponding to the emission of the $Cs_3Cu_2I_5$ phase, the PLE spectra end at ~320 nm. However, the PLE spectra end at ~350 nm for the excitation spectra monitored at 580 nm corresponding to the emission of the $CsCu_2I_3$ phase. The characteristic of PL peak-dependent-PLE is advantageous for the PL modulation via simply changing the excitation wavelengths. Specifically, the $Cs_3Cu_2I_5$ phase in the composite film can be effectively stimulated under an excitation wavelength of 300 nm or shorter, which leads to an independent single peak located at 441 nm. Although the $CsCu_2I_3$ phase can also be stimulated under the same conditions, the yellow emission resulting from the $CsCu_2I_3$ phase does not appear. The reasons can be explained as follows: on

24 December 2023 15:22:00

© Author(s) 2023

the one hand, a PLE intensity of 580 nm is lower than that of 441 nm under an excitation wavelength of 300 nm or shorter; on the other hand, the PLQY of $CsCu_2I_3$ is much lower than that of $Cs_3Cu_2I_5$ (Fig. S2), due to the low self-trapping state depth, thus, leading to the higher de-trapping rate of the trapped excitons in the $CsCu_2I_3$ film. When the excitation wavelength is increased to 310 nm, the yellow emission originating from the $CsCu_2I_3$ phase appears gradually, which results in the white emission in combination with the blue emission of the $Cs_3Cu_2I_5$ phase. Although an PLE intensity of 450 nm is pretty low under an excitation wavelength of 310 nm, the blue emission intensity of the $Cs_3Cu_2I_5$ phase is still high, which is attributed to the high PLQY of $Cs_3Cu_2I_5$. The high PLQY is associated with the unique zero-dimensional structure of $Cs_3Cu_2I_5$, which leads to the easy formation of excitons due to the strong Coulomb effect between the photoexcited electrons and holes.[34] When the excitation wavelength is further increased to 320 nm, the yellow emission of the $CsCu_2I_3$ phase increases gradually, while the blue emission of $Cs_3Cu_2I_5$ phase gradually weakens and eventually disappears. The disappearance of blue emission of the $Cs_3Cu_2I_5$ phase is due to a low PLE intensity of 450 nm under an excitation wavelength of 320 nm, indicating the $Cs_3Cu_2I_5$ phase cannot be effectively stimulated. Meanwhile, the excitation wavelength-dependent PL spectra and emission wavelength-dependent PLE spectra of pure $CsCu_2I_3$ and $Cs_3Cu_2I_5$ show different excitation spectral range and no excitation-dependent emission features (Fig. S3).

We conducted time-resolved photoluminescence (TRPL) measurements to study the exciton dynamics of the $CsCu_2I_3$@$Cs_3Cu_2I_5$ composite film. The TRPL spectra under the excitation wavelengths of 300 and 320 nm are fitted by the single-exponential equation as follows:[35]

$$f(t) = A\exp(-t/\tau). \quad (1)$$

The τ lifetimes are 1.37, 1.424, and 1.416 μs for $Cs_3Cu_2I_5$ under 300, 310, and 320 nm, respectively [Figs. S4(a)–S4(c)]. For the $CsCu_2I_3$ phase, the τ lifetimes are 1.424, 1.307, and 1.411 μs under 300, 310, and 320 nm, respectively [Figs. S4(d)–S4(f)]. Different from the triple-mode anti-counterfeiting materials with afterglow,[18] the fluorescence lifetime of $CsCu_2I_3$@$Cs_3Cu_2I_5$ (Fig. S5) is far less than the time that human eyes can distinguish (~20 ms), so the fast switch among three luminous modes can be realized.

Generally, such an extremely long lifetime and broadband PL emission imply that the emission of the $CsCu_2I_3$@$Cs_3Cu_2I_5$ composite film does not result from the band-edge related recombination but may be caused by the self-trapped excitons (STEs).[36] In order to gain in-depth insights into the STEs dynamics and exciton–phonon interaction, the temperature-dependent PL measurements were conducted under an excitation wavelength of 300 and 320 nm, in which the $Cs_3Cu_2I_5$ and $CsCu_2I_3$ phases can be stimulated, respectively. With the increase of the temperature from 80 to 300 K, a strong thermal quenching behavior of the PL intensity can be observed because the thermal de-trapping process becomes non-negligible in the high-temperature region; thus, the non-radiative loss gradually dominates the STEs dynamics [Figs. 3(a) and 3(d)]. In addition, the blue emission under 300 nm UV light (next called

24 December 2023 15:22:00

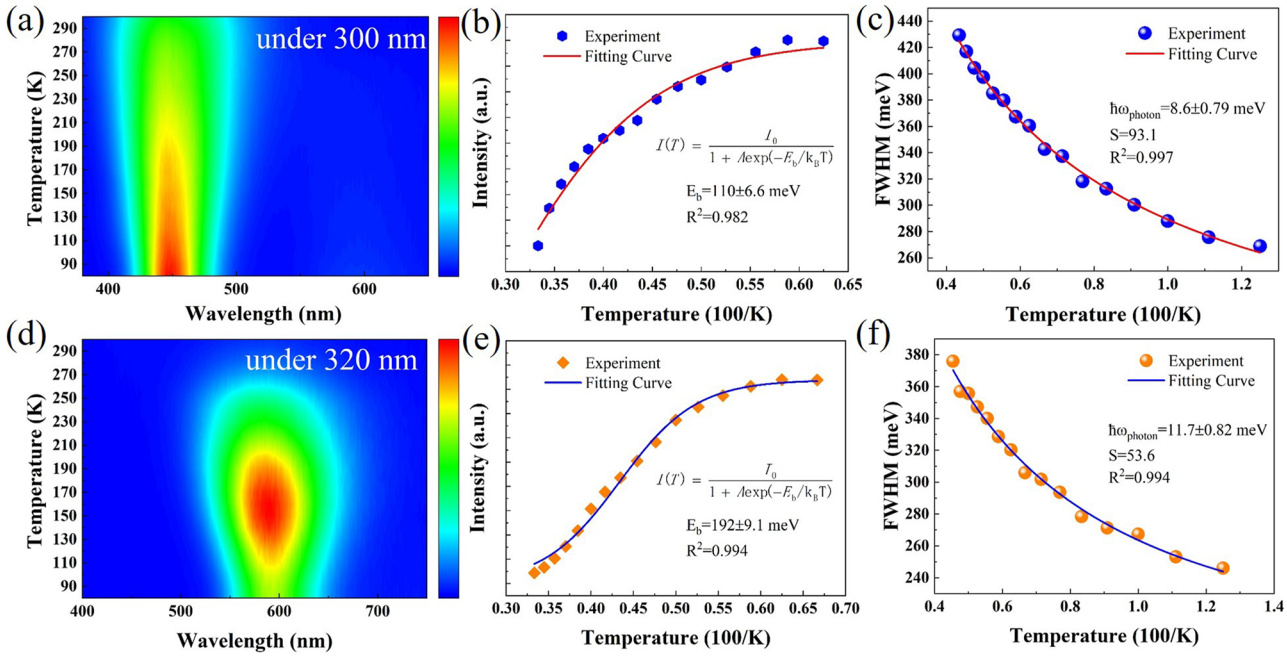


FIG. 3. (a) Simulation of temperature-dependent PL spectra under 300 nm wavelength excitation. (b) Integrated PL intensity and (c) FWHM of the $CsCu_2I_3$@$Cs_3Cu_2I_5$ films under 300 nm wavelength excitation as a function of reciprocal temperature. (d) Simulation of temperature-dependent PL spectra under 320 nm wavelength excitation. (e) Integrated PL intensity and (f) FWHM of the $CsCu_2I_3$@$Cs_3Cu_2I_5$ films under 320 nm wavelength excitation as a function of reciprocal temperature.

© Author(s) 2023

STE_B) keeps almost unchanged, while the yellow emission under 320 nm UV light (STE_Y) presents a continuous blue-shift trend. Such an abnormal blue-shift phenomenon could be attributed to the thermal expansion of the lattice and the electron–phonon renormalization in the case of $CsCu_2I_3$.[34] Figures 3(b) and 3(e) show the Arrhenius plots of the integrated PL intensity for the case excited by 300 and 320 nm, respectively, and the thermal quenching behavior can be well fitted by the following formula:[37,38]

$$I(T) = \frac{I_0}{1 + A\exp\left(-\frac{E_b}{k_b T}\right)}, \quad (2)$$

where I_0 is the emission intensity at 0 K, A is a proportional constant, E_b is the exciton binding energy, T is the temperature, and k_b is the Boltzmann constant. The fitting curves indicate that the E_b of STE_B and STE_Y are about 110 and 192 meV, respectively. Moreover, R^2 is the error of data fitting, indicating the reliability of the fitting results. Such a high E_b suggests that the PL emission of $CsCu_2I_3$@$Cs_3Cu_2I_5$ mainly originates from the exciton recombination rather than the recombination of the free electrons and holes, which favors an efficient radiative recombination process. The exciton is supposed to be localized around $[Cu_xI_y]$ to form STEs through a strong Coulomb effect.[34,39]

Generally, the broadening of exciton emission linewidth with the increase of temperature is attributed to the exciton binding fluctuation arising from the atoms' vibration in the crystal.[34] The relationship between the temperature and FWHM is determined by the strength of electron–photon coupling. Therefore, the Huang–Rhys factor (S) and the photon frequency ($\hbar\omega_{photon}$) are investigated to reveal the electron–photon coupling using the following equation:[40]

$$FWHM(T) = 2.36\sqrt{S}\,\hbar\omega_{photon}\sqrt{\coth\frac{\hbar\omega_{photon}}{2k_bT}}, \quad (3)$$

where ω_{photon} is the frequency of phonon mode and $\hbar$ is the Planck constant. Through fitting the temperature-dependent FWHM curve, the value of the S factor is extracted as 93.1 and 53.6 for $Cs_3Cu_2I_5$ and $CsCu_2I_3$ phases, respectively. The $\hbar\omega_{photon}$ is extracted as 8.6 and 11.7 meV for $Cs_3Cu_2I_5$ and $CsCu_2I_3$ phases, respectively, as shown in Figs. 3(c) and 3(f). The Huang–Rhys parameter (S) indicates the distortion degree of the self-trapped state with respect to the ground state. Such an S factor is much higher than that of many traditional materials with band-edge luminescent features, which manifests in the presence of a strong electron–photon coupling in $CsCu_2I_3$@$Cs_3Cu_2I_5$ and facilitates the formation of STEs.[41–43] It is noted that the different local dimensions of Cu sites in the crystal structure give rise to different origins for the STEs of $Cs_3Cu_2I_5$ and $CsCu_2I_3$, in which the local dimension of Cu sites in the $[Cu_2I_5]^{3-}$ cluster is obviously lower than that of the $[Cu_2I_3]^-$ chain [Figs. S6(a) and S6(b)].[34] Therefore, the STEs emission shows an expected structure-oriented effect. Moreover, we measured the emission intensity-excitation power characteristic of $CsCu_2I_3$@$Cs_3Cu_2I_5$ to exclude the possibility of defect-induced emission [Fig. S6(c)], which typically leads to fast intensity saturation with the increase of excitation power.[36] The corresponding photophysical processes can be described using a configuration coordinate diagram [Fig. S6(d)], and the density functional theory (DFT) calculation results of $CsCu_2I_3$ and $Cs_3Cu_2I_5$ are shown in Fig. S7. The calculation value of the bandgap for $CsCu_2I_3$ and $Cs_3Cu_2I_5$ is 1.9 and 2.6 eV, respectively, which is consistent with the previous report using generalized gradient approximation Perdew–Burke–Ernzerhof (GGA-PBE) functionals [Figs. S7(a) and S7(b)].[30,34,44] The experimental bandgaps of $CsCu_2I_3$ and $Cs_3Cu_2I_5$ are 3.73 and 4.06 eV inferred from the Tauc plots [Figs. S7(e) and S7(f)]. It is noted that the calculated bandgap is smaller than the experimental value because of the discontinuity of exchange correlation energy, which may cause the bandgap to be underestimated by 30%–50%.[45,46] It is well known that the material stability is of great importance for its practical application in anti-counterfeiting. We further prepared the $CsCu_2I_3$@$Cs_3Cu_2I_5$@PEO composites by adding PEO to the precursor solution of $CsCu_2I_3$@$Cs_3Cu_2I_5$. The reasons for selecting PEO can be accounted for as follows: first, PEO is transparent and easily dissolved in dimethyl sulfoxide (DMSO)/DMF solution; second, PEO has a positive effect on film uniformity (Fig. S8); and third, PEO has the advantages of excellent thermal, oxygen, and moisture stability. Mechanistically, the C–O group on PEO was expected to interact with Cu^+ from $CsCu_2I_3$@$Cs_3Cu_2I_5$, which can passivate the anion vacancies. Moreover, the hygroscopic polymer strongly slows down the hydration process by absorbing water. Benefiting from these two positive effects, the addition of PEO will enhance the morphology and stability of $CsCu_2I_3$@$Cs_3Cu_2I_5$.[47–52] In order to assess the effect of PEO on the thermal stability of $CsCu_2I_3$@$Cs_3Cu_2I_5$, the thermal cycling test (280–440–280 K) was performed in ambient air, and the absolute PLQY was tracked at 280 K [Fig. 4(a)]. The initial PLQY of $CsCu_2I_3$@$Cs_3Cu_2I_5$ without PEO is 51.07% [Fig. S9(a)], while that of $CsCu_2I_3$@$Cs_3Cu_2I_5$ with PEO, hereafter called "$CsCu_2I_3$@$Cs_3Cu_2I_5$@PEO," is 50.67% [Fig. S9(c)], indicating that PEO has nearly no influence on the PL efficiency. After ten cycles of the continuous test, the PLQY of the $CsCu_2I_3$@$Cs_3Cu_2I_5$ sample shows 17.2% decrease, while that of the $CsCu_2I_3$@$Cs_3Cu_2I_5$@PEO sample shows a slightly lower decrease of 14.9%, revealing enhanced thermal stability upon the incorporation of PEO [Figs. S9(b) and S9(d)].

To explore the effect of PEO on the stability against oxygen and moisture, the time-dependent PL spectra of both samples were measured under ambient conditions (18–20 °C, 30%–40% humidity), as shown in Fig. 4(b). After 30 days of storage, the $CsCu_2I_3$@$Cs_3Cu_2I_5$@PEO sample still retains about 95% of its initial PL intensity, while the $CsCu_2I_3$@$Cs_3Cu_2I_5$ sample retains about 89% of its initial PL intensity. Figures 4(c) and 4(d) show the pseudocolor map of PL spectra monitored when the samples were exposed to 310 nm UV light. It can be found that the $CsCu_2I_3$@$Cs_3Cu_2I_5$ sample exhibits more severe emission quenching of the $CsCu_2I_3$ phase, i.e., the CIE change is 25.8% from (0.3197, 0.3057) to (0.25, 0.2143) compared with 3.5% of the $CsCu_2I_3$@$Cs_3Cu_2I_5$@PEO sample from (0.2888, 0.2757) to (0.2804, 0.2642), manifesting that the PEO helps for enhanced stability against UV exposure [Figs. 4(e) and 4(f)]. Meanwhile, the PL spectra of the samples exposed to 300 and 320 nm UV were measured to verify the stability improvement against UV light upon the incorporation of PEO (Fig. S10). The stability test of the sample under UV light was carried out, and the corresponding results are shown in Fig. S11. After a continuous irradiation of 200 h, the PL intensity remains at 86.7% of the maximum. These results indicate that the incorporation of PEO improves the stability of $CsCu_2I_3$@$Cs_3Cu_2I_5$ against high temperature, oxygen, moisture, and

24 December 2023 15:22:00

© Author(s) 2023

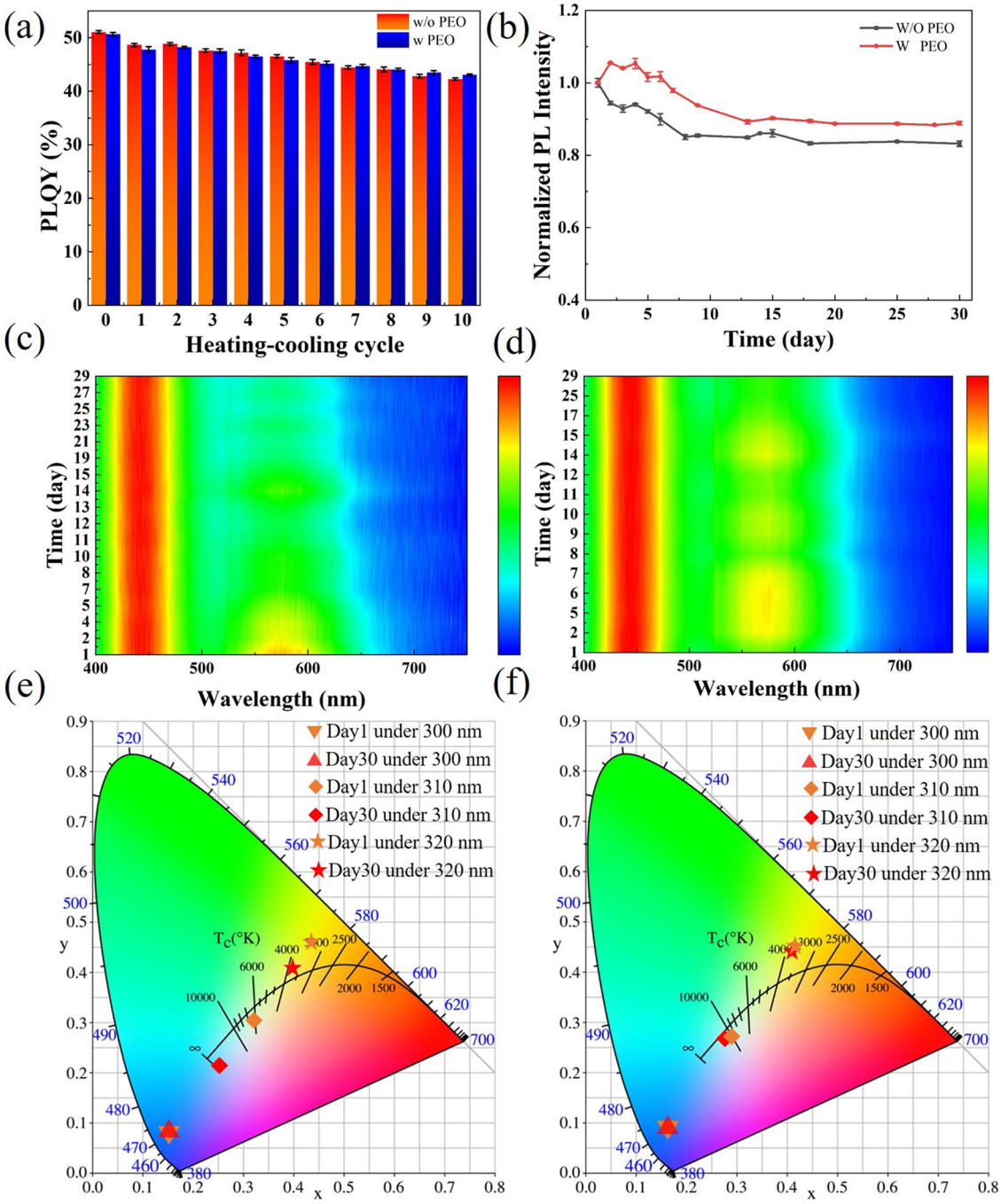


FIG. 4. (a) PLQY test with heating–cooling cycle (the samples were heated on a hotplate at 440 K for 15 min and, then, measured after cooling down to 280 K). (b) PL intensity of $CsCu_2I_3$@$Cs_3Cu_2I_5$ and $CsCu_2I_3$@$Cs_3Cu_2I_5$@PEO measured in air. PL spectra evolution of the (c) control sample and (d) PEO sample at different storage periods in ambient air. CIE of the (e) control sample and (f) PEO sample.

UV exposure, which is beneficial for extending the application durability in a much harsher environment. It is worth noting that the stability of $CsCu_2I_3$@$Cs_3Cu_2I_5$@PEO is superior to that of previously reported perovskite-based anti-counterfeiting materials (Table S1).

The unique emissive properties and excellent stability of the $CsCu_2I_3$@$Cs_3Cu_2I_5$@PEO make it promising for application in advanced anti-counterfeiting, considering that few alternatives with triple-mode emission have been reported so far. As a

24 December 2023 15:22:00

© Author(s) 2023



FIG. 5. Application of the $CsCu_2I_3$@$Cs_3Cu_2I_5$ composite as a triple-mode anti-counterfeiting ink. (a)–(d) The "SEU" pattern printed by $CsCu_2I_3$@$Cs_3Cu_2I_5$@PEO. (e)–(h) The "SEU" pattern printed by $Cs_3Cu_2I_5$, $CsCu_2I_3$@$Cs_3Cu_2I_5$@PEO, and $CsCu_2I_3$, respectively. (i)–(l) QR code of $CsCu_2I_3$@$Cs_3Cu_2I_5$ on glass under different lights.

preliminary demonstration of the practical application of $CsCu_2I_3$@$Cs_3Cu_2I_5$@PEO in anti-counterfeiting, the $CsCu_2I_3$@$Cs_3Cu_2I_5$@PEO pattern is transferred onto a piece of paper by using a micro-structured stamp. As shown in Fig. 5(a), the $CsCu_2I_3$@$Cs_3Cu_2I_5$@PEO is colorless, and the pattern is hidden. Under an excitation of 300 nm, the pattern "SEU" appears with blue emission, since $Cs_3Cu_2I_5$ is effectively stimulated [Fig. 5(b)]. When the excitation light is switched from 300 to 310 nm, the color of "SEU" is changed to white, due to the combination of blue and yellow emission, originating from $Cs_3Cu_2I_5$ and $CsCu_2I_3$ phases, respectively [Fig. 5(c)]. The color of "SEU" is eventually changed to yellow when adjusting the excitation wavelength to 320 nm, at which $CsCu_2I_3$ is effectively stimulated [Fig. 5(d)].

Combined with different phases of luminescent materials, the triple-mode anti-counterfeiting is further demonstrated in Figs. 5(e)–5(h) and video (supplementary material), where the "SEU" pattern is printed by $Cs_3Cu_2I_5$, $CsCu_2I_3$@$Cs_3Cu_2I_5$@PEO, and $CsCu_2I_3$, respectively. In order to demonstrate the intricate pattern applications of $CsCu_2I_3$@$Cs_3Cu_2I_5$@PEO on various substrates, the anti-counterfeiting materials are transferred onto the glass. The $CsCu_2I_3$@$Cs_3Cu_2I_5$@PEO on the glass is colorless and transparent under indoor light. On the contrary, under different UV irradiations (e.g., 300, 310, and 320 nm), the QR code shows triple-mode PL emission and can be easily scanned [Figs. 5(i)–5(l)].

CONCLUSION

In summary, we have demonstrated a triple-color fluorescence of lead-free copper-based halides $CsCu_2I_3$@$Cs_3Cu_2I_5$ composite and its application in advanced anti-counterfeiting. The triple-mode PL emission originated from the structure-oriented self-trapped excitons (STEs) effect of $Cs_3Cu_2I_5$ and $CsCu_2I_3$ phases, which features the broadband emission and long lifetime of exciton. The composite exhibits a bright blue emission from the $Cs_3Cu_2I_5$ phase under 300 nm or shorter excitation wavelengths, while the $CsCu_2I_3$ phase cannot be stimulated. As the excitation wavelength switches from 300 to 310 nm, a yellow emission from the $CsCu_2I_3$ phase emerges, leading to a white emission with the $Cs_3Cu_2I_5$ and $CsCu_2I_3$ phases excited simultaneously. With the excitation wavelength further increased to 320 nm, the pure yellow emission can be obtained with the $CsCu_2I_3$ phase excited, while the blue emission of the $Cs_3Cu_2I_5$ phase is suppressed. Importantly, with the incorporation of PEO, the $CsCu_2I_3$@$Cs_3Cu_2I_5$@PEO exhibits excellent stability against high temperatures, oxygen, moisture, and UV exposure, which is of great importance to its application in advanced anti-counterfeiting.

SUPPLEMENTARY MATERIAL

See the supplementary material for experiment details, PLQY, PLE, TRPL, density functional theory calculation, and SEM results.

ACKNOWLEDGMENTS

This paper was supported by the National Natural Science Foundation Project of China (Grant Nos. 62205153 and 62205152), the Jiangsu Province Basic Research Program (Grant No. BK20212006), Ministry of Science and Technology International

24 December 2023 15:22:00

© Author(s) 2023

cooperation projects (Grant No. 2021YFE0105900), the Natural Science Foundation of Jiangsu Province (Grant No. BK20190774), the Anhui Province Key Laboratory of Optoelectric Materials Science and Technology (Grant No. OMST202106), the National Key Research and Development Program of China (Grant Nos. 2018YFE0125500 and 2021YFE0105900), the National Natural Science Foundation Project for Young Researcher (Grant No. 12005038), the Research Fund for International Young Scientists (Grant No. 62050410350), the National Natural Science Foundation Project of China (Grant Nos. 62175028, 51879042, and 61674029), Program 111_2.0 in China (Grant No. BP0719013), and Leading Technology of the Jiangsu Basic Research Plan (Grant No. BK20192003). D.Z. acknowledges the financial support from the Fundamental Research Funds for the Central Universities (Grant No. YJ201955) and the Engineering Featured Team Fund of Sichuan University (Grant No. 2020SCUNG102).

AUTHOR DECLARATIONS

Conflict of Interest

The authors have no conflicts to disclose.

Author Contributions

J.P., L.M., Y.H., B.W., and C. Lin led the device physics work. J.C. and D.Z. led the materials chemistry work. C. Liu synthesized and optimized the materials. Zihan Zhao, L.W., F.F., W.L., and Q.L. conducted the optical measurements and analyzed the optical properties. C. Liu, Y.Z., and M.L. validate and visualize the data. Q.L., Zhiwei Zhao, J.W., Zhuoya Zhu, and M.E. provide the resources and administrate projects. C. Liu carried out the device fabrication and characterizations. C. Liu wrote the first draft of the manuscript. J.C., W.L., X.Z., and D.Z. provided major revisions. All authors discussed the results and commented on the manuscript. J.C. and D.Z. supervised the project.

Chengjun Liu: Conceptualization (equal); Data curation (equal); Methodology (equal); Software (equal); Visualization (equal); Writing – original draft (equal). **Yuyi Zhang**: Conceptualization (equal); Investigation (equal); Software (equal). **Manman Luo**: Conceptualization (supporting); Data curation (supporting); Investigation (supporting). **Lixi Wang**: Investigation (supporting); Methodology (supporting); Supervision (supporting). **Xingyu Liu**: Data curation (supporting); Formal analysis (supporting); Supervision (supporting). **Jiangyong Pan**: Methodology (supporting); Writing – original draft (supporting); Writing – review & editing (supporting). **Zihan Zhao**: Data curation (supporting); Formal analysis (supporting). **Fan Fang**: Data curation (supporting); Investigation (supporting); Visualization (supporting). **Lei Mao**: Methodology (supporting); Visualization (supporting). **Yuling Huang**: Software (supporting); Visualization (supporting). **Bingqi Wang**: Supervision (supporting); Visualization (supporting). **Congyuan Lin**: Investigation (supporting); Visualization (supporting). **Wei Lei**: Conceptualization (supporting); Funding acquisition (equal); Software (supporting). **Qing Li**: Project administration (supporting). **Zhiwei Zhao**: Project administration (supporting); Supervision (supporting). **Jun Wu**: Project administration (supporting); Supervision (supporting). **Zhuoya Zhu**: Project administration (supporting); Supervision (supporting). **Mehmet Ertugrul**: Project administration (supporting); Supervision (supporting). **Xiaobing Zhang**: Funding acquisition (equal); Project administration (equal); Writing – review & editing (supporting). **Jing Chen**: Funding acquisition (equal); Writing – review & editing (equal). **Dewei Zhao**: Conceptualization (equal); Visualization (equal); Writing – review & editing (equal).

DATA AVAILABILITY

The data that support the findings of this study are available from the corresponding authors upon reasonable request.

REFERENCES

[1] M. Tan, F. Li, X. Wang, R. Fan, and G. Chen, "Temporal multilevel luminescence anticounterfeiting through scattering media," ACS Nano **14**(6), 6532–6538 (2020).
[2] M.-K. Tsang, G. Bai, and J. Hao, "Stimuli responsive upconversion luminescence nanomaterials and films for various applications," Chem. Soc. Rev. **44**(6), 1585–1607 (2015).
[3] W. Ren, G. Lin, C. Clarke, J. Zhou, and D. Jin, "Optical nanomaterials and enabling technologies for high-security-level anticounterfeiting," Adv. Mater. **32**(18), 1901430 (2020).
[4] Y. Gu, C. He, Y. Zhang, L. Lin, B. D. Thackray, and J. Ye, "Gap-enhanced Raman tags for physically unclonable anticounterfeiting labels," Nat. Commun. **11**(1), 516 (2020).
[5] W. Hong, Z. Yuan, and X. Chen, "Structural color materials for optical anticounterfeiting," Small **16**(16), 1907626 (2020).
[6] D. Li, L. Tang, J. Wang, X. Liu, and Y. Ying, "Multidimensional SERS barcodes on flexible patterned plasmonic metafilm for anticounterfeiting applications," Adv. Opt. Mater. **4**(10), 1475–1480 (2016).
[7] J. Liu, H. Rijckaert, M. Zeng, K. Haustraete, B. Laforce, L. Vincze, I. Van Driessche, A. M. Kaczmarek, and R. Van Deun, "Simultaneously excited downshifting/upconversion luminescence from lanthanide-doped core/shell fluoride nanoparticles for multimode anticounterfeiting," Adv. Funct. Mater. **28**(17), 1707365 (2018).
[8] X. Yu, H. Zhang, and J. Yu, "Luminescence anti-counterfeiting: From elementary to advanced," Aggregate **2**(1), 20–34 (2021).
[9] A. M. Kaczmarek, Y.-Y. Liu, C. Wang, B. Laforce, L. Vincze, P. Van Der Voort, K. Van Hecke, and R. Van Deun, "Lanthanide 'chameleon' multistage anti-counterfeit materials," Adv. Funct. Mater. **27**(20), 1700258 (2017).
[10] S. Han, H. J. Bae, J. Kim, S. Shin, S.-E. Choi, S. H. Lee, S. Kwon, and W. Park, "Lithographically encoded polymer microtaggant using high-capacity and error-correctable QR code for anti-counterfeiting of drugs," Adv. Mater. **24**(44), 5924–5929 (2012).
[11] M. Ataeefard and F. Nourmohammadian, "Producing fluorescent digital printing ink: Investigating the effect of type and amount of coumarin derivative dyes on the quality of ink," J. Lumin. **167**, 254–260 (2015).
[12] L. Xu, J. Chen, J. Song, J. Li, J. Xue, Y. Dong, B. Cai, Q. Shan, B. Han, and H. Zeng, "Double-protected all-inorganic perovskite nanocrystals by crystalline matrix and silica for triple-modal anti-counterfeiting codes," ACS Appl. Mater. Interfaces **9**(31), 26556–26564 (2017).
[13] D. Zhang, W. Zhou, Q. Liu, and Z. Xia, "$CH_3NH_3PbBr_3$ perovskite nanocrystals encapsulated in lanthanide metal-organic frameworks as a photoluminescence converter for anti-counterfeiting," ACS Appl. Mater. Interfaces **10**(33), 27875–27884 (2018).
[14] R. Liu, W. Zhang, G. Li, and W. Liu, "An ultraviolet excitation anti-counterfeiting material of Sb^{3+} doped Cs_2ZrCl_6 vacancy-ordered double perovskite," Inorg. Chem. Front. **8**(17), 4035–4043 (2021).
[15] Z. Zeng, B. Huang, X. Wang, L. Lu, Q. Lu, M. Sun, T. Wu, T. Ma, J. Xu, Y. Xu, S. Wang, Y. Du, and C. H. Yan, "Multimodal luminescent $Yb^{3+}/Er^{3+}/Bi^{3+}$-doped

24 December 2023 15:22:00

© Author(s) 2023

perovskite single crystals for X-ray detection and anti-counterfeiting," Adv. Mater. **32**(43), 2004506 (2020).
[16]Z. Wang, Y. Zhang, X. Liu, Y. Yu, F. Xu, J. Ding, X. Liang, K. Yang, and W. Xiang, "High stability and strong luminescence $CsPbBr_3/Cs_4PbBr_6$ perovskite nanocomposite: Large-scale synthesis, reversible luminescence, and anti-counterfeiting application," Adv. Mater. Technol. **6**(12), 2100654 (2021).
[17]X. Li, S. Xu, F. Liu, J. Qu, H. Shao, Z. Wang, Y. Cui, D. Ban, and C. Wang, "Bi and Sb codoped $Cs_2Ag_{0.1}Na_{0.9}InCl_6$ double perovskite with excitation-wavelength-dependent dual-emission for anti-counterfeiting application," ACS Appl. Mater. Interfaces **13**(26), 31031–31037 (2021).
[18]Z. Wang, P. Pei, D. Bai, S. Zhao, X. Ma, and W. Liu, "Multicolor luminescence and triple-mode emission of simple $CaTiO_3:Pr^{3+},Er^{3+}$ particles for advanced anti-counterfeiting," Inorg. Chem. Front. **7**(13), 2506–2514 (2020).
[19]J. Lin, C. Yang, P. Huang, S. Wang, M. Liu, N. Jiang, and D. Chen, "Photoluminescence tuning from glass-stabilized $CsPbX_3$ (X = Cl, Br, I) perovskite nanocrystals triggered by upconverting Tm: KYb_2F_7 nanoparticles for high-level anti-counterfeiting," Chem. Eng. J. **395**, 125214 (2020).
[20]W. Hu, T. Li, X. Liu, D. Dastan, K. Ji, and P. Zhao, "1550 nm pumped upconversion chromaticity modulation in Er^{3+} doped double perovskite $LiYMgWO_6$ for anti-counterfeiting," J. Alloys Compd. **818**, 152933 (2020).
[21]F. Zhang, W. Liang, L. Wang, Z. Ma, X. Ji, M. Wang, Y. Wang, X. Chen, D. Wu, X. Li, Y. Zhang, C. Shan, and Z. Shi, "Moisture-induced reversible phase conversion of cesium copper iodine nanocrystals enables advanced anti-counterfeiting," Adv. Funct. Mater. **31**(47), 2105771 (2021).
[22]W. Cui, J. Zhao, L. Wang, P. Lv, X. Li, Z. Yin, C. Yang, and A. Tang, "Unraveling the phase transition and luminescence tuning of Pb-free Cs–Cu–I perovskites enabled by reaction temperature and polar solvent," J. Phys. Chem. Lett. **13**(22), 4856–4863 (2022).
[23]Z. Ma, X. Ji, M. Wang, F. Zhang, Z. Liu, D. Yang, M. Jia, X. Chen, D. Wu, Y. Zhang, X. Li, Z. Shi, and C. Shan, "Carbazole-containing polymer-assisted trap passivation and hole-injection promotion for efficient and stable $CsCu_2I_3$-based yellow LEDs," Adv. Sci. **9**, 2202408 (2022).
[24]K.-X. Xu, Z. Zhou, and J. Zhang, "Phonon-assisted upconversion photoluminescence of a self-trapped exciton in the Rb_2CuCl_3 single crystal," J. Phys. Chem. Lett. **14**(1), 32–37 (2023).
[25]J. Lv, X. Lu, X. Li, M. Xu, J. Zhong, X. Zheng, Y. Shi, X. Zhang, and Q. Zhang, "Epitaxial growth of lead-free 2D $Cs_3Cu_2I_5$ perovskites for high-performance UV photodetectors," Small **18**(27), 2201715 (2022).
[26]H. Chen, L. Zhu, C. Xue, P. Liu, X. Du, K. Wen, H. Zhang, L. Xu, C. Xiang, C. Lin, M. Qin, J. Zhang, T. Jiang, C. Yi, L. Cheng, C. Zhang, P. Yang, M. Niu, W. Xu, J. Lai, Y. Cao, J. Chang, H. Tian, Y. Jin, X. Lu, L. Jiang, N. Wang, W. Huang, and J. Wang, "Efficient and bright warm-white electroluminescence from lead-free metal halides," Nat. Commun. **12**(1), 1421 (2021).
[27]L. Wang, Z. Shi, Z. Ma, D. Yang, F. Zhang, X. Ji, M. Wang, X. Chen, G. Na, S. Chen, D. Wu, Y. Zhang, X. Li, L. Zhang, and C. Shan, "Colloidal synthesis of ternary copper halide nanocrystals for high-efficiency deep-blue light-emitting diodes with a half-lifetime above 100 h," Nano Lett. **20**(5), 3568–3576 (2020).
[28]Z. Ma, Z. Shi, D. Yang, Y. Li, F. Zhang, L. Wang, X. Chen, D. Wu, Y. Tian, Y. Zhang, L. Zhang, X. Li, and C. Shan, "High color-rendering index and stable white light-emitting diodes by assembling two broadband emissive self-trapped excitons," Adv. Mater. **33**(2), 2001367 (2021).
[29]C. Zou, Q. Liu, K. Chen, F. Chen, Z. Zhao, Y. Cao, C. Deng, X. Wang, X. Li, S. Zhan, F. Gao, and S. Li, "A high-performance polarization-sensitive and stable self-powered UV photodetector based on a dendritic crystal lead-free metal-halide $CsCu_2I_3$/GaN heterostructure," Mater. Horiz. **9**(5), 1479–1488 (2022).
[30]J. Yang, W. Kang, Z. Liu, M. Pi, L.-B. Luo, C. Li, H. Lin, Z. Luo, J. Du, M. Zhou, and X. Tang, "High-performance deep ultraviolet photodetector based on a one-dimensional lead-free halide perovskite $CsCu_2I_3$ film with high stability," J. Phys. Chem. Lett. **11**(16), 6880–6886 (2020).
[31]X. Zhou, C. Wang, J. Luo, L. Zhang, F. Zhao, and Q. Ke, "High-performance self-powered UV photodetector based on CuI/$CsCu_2I_3$/GaN heterojunction," Chem. Eng. J. **450**, 136364 (2022).
[32]K. Zhang, S. Wang, and L. Yi, "Defect emission in $Cs_3Cu_2I_5$ and $CsCu_2I_3$ halide films," J. Lumin. **254**, 119516 (2023).
[33]M. Li, C. Cao, W. Liu, N. Wang, C. Yi, R. Li, and J. Wang, "Orientation regulation of one-dimensional $CsCu_2I_3$ perovskites for visible-blind ultraviolet photodetectors," J. Phys. Chem. Lett. **13**(28), 6462–6467 (2022).
[34]R. Lin, Q. Zhu, Q. Guo, Y. Zhu, W. Zheng, and F. Huang, "Dual self-trapped exciton emission with ultrahigh photoluminescence quantum yield in $CsCu_2I_3$ and $Cs_3Cu_2I_5$ perovskite single crystals," J. Phys. Chem. C **124**(37), 20469–20476 (2020).
[35]C. Liu, L. Wang, F. Fang, Z. Zhao, J. Pan, J. Akram, S. B. Shafie, R. Z. Talaighil, Q. Li, Z. Zhao, J. Wu, Z. Zhu, W. Lei, X. Zhang, and J. Chen, "Energy down-conversion $Cs_3Cu_2Cl_5$ nanocrystals for boosting the efficiency of UV photodetector," Front. Mater. **8**, 682833 (2021).
[36]H. Chen, J. M. Pina, F. Yuan, A. Johnston, D. Ma, B. Chen, Z. Li, A. Dumont, X. Li, Y. Liu, S. Hoogland, Z. Zajacz, Z. Lu, and E. H. Sargent, "Multiple self-trapped emissions in the lead-free halide $Cs_3Cu_2I_5$," J. Phys. Chem. Lett. **11**(11), 4326–4330 (2020).
[37]S. Zott, K. Leo, M. Ruckh, and H.-W. Schock, "Radiative recombination in $CuInSe_2$ thin films," J. Appl. Phys. **82**(1), 356–367 (1997).
[38]D. S. Jiang, H. Jung, and K. Ploog, "Temperature dependence of photoluminescence from GaAs single and multiple quantum-well heterostructures grown by molecular-beam epitaxy," J. Appl. Phys. **64**(3), 1371–1377 (1988).
[39]Z. Ma, Z. Shi, C. Qin, M. Cui, D. Yang, X. Wang, L. Wang, X. Ji, X. Chen, J. Sun, D. Wu, Y. Zhang, X. J. Li, L. Zhang, and C. Shan, "Stable yellow light-emitting devices based on ternary copper halides with broadband emissive self-trapped excitons," ACS Nano **14**(4), 4475–4486 (2020).
[40]W. Stadler, D. M. Hofmann, H. C. Alt, T. Muschik, B. K. Meyer, E. Weigel, G. Müller-Vogt, M. Salk, E. Rupp, and K. W. Benz, "Optical investigations of defects in $Cd_{1-x}Zn_xTe$," Phys. Rev. B **51**(16), 10619–10630 (1995).
[41]M. D. Smith and H. I. Karunadasa, "White-light emission from layered halide perovskites," Acc. Chem. Res. **51**(3), 619–627 (2018).
[42]R. Lin, Q. Guo, Q. Zhu, Y. Zhu, W. Zheng, and F. Huang, "All-inorganic $CsCu_2I_3$ single crystal with high-PLQY (≈15.7%) intrinsic white-light emission via strongly localized 1D excitonic recombination," Adv. Mater. **31**(46), 1905079 (2019).
[43]J. Luo, M. Hu, G. Niu, and J. Tang, "Lead-free halide perovskites and perovskite variants as phosphors toward light-emitting applications," ACS Appl. Mater. Interfaces **11**(35), 31575–31584 (2019).
[44]F. Gao, X. Zhu, Q. Feng, W. Zhong, W. Liu, H. Xu, and Y. Liu, "Deep-blue emissive $Cs_3Cu_2I_5$ perovskites nanocrystals with 96.6% quantum yield via InI_3-assisted synthesis for light-emitting device and fluorescent ink applications," Nano Energy **98**, 107270 (2022).
[45]F. Aryasetiawan and O. Gunnarsson, "The GW method," Rep. Prog. Phys. **61**, 237–312 (1998).
[46]M. Ernzerhof and G. E. Scuseria, "Assessment of the Perdew–Burke–Ernzerhof exchange-correlation functional," J. Chem. Phys. **110**(11), 5029–5036 (1999).
[47]J. Li, X. Shan, S. G. R. Bade, T. Geske, Q. Jiang, X. Yang, and Z. Yu, "Single-layer halide perovskite light-emitting diodes with sub-band gap turn-on voltage and high brightness," J. Phys. Chem. Lett. **7**(20), 4059–4066 (2016).
[48]Y. Tian, C. Zhou, M. Worku, X. Wang, Y. Ling, H. Gao, Y. Zhou, Y. Miao, J. Guan, and B. Ma, "Highly efficient spectrally stable red perovskite light-emitting diodes," Adv. Mater. **30**(20), 1707093 (2018).
[49]J. Li, S. G. R. Bade, X. Shan, and Z. Yu, "Single-layer light-emitting diodes using organometal halide perovskite/poly(ethylene oxide) composite thin films," Adv. Mater. **27**(35), 5196–5202 (2015).
[50]J. Zhang, H. Wang, F. Cao, S. Wang, J. Wu, Y. Dou, J. Zhang, J. Chen, D. Zhao, and X. Yang, "Efficient all-solution-processed perovskite light-emitting diodes enabled by small-molecule doped electron injection layers," Adv. Opt. Mater. **8**(2), 1900567 (2019).
[51]Z. Wang, F. Wang, W. Sun, R. Ni, S. Hu, J. Liu, B. Zhang, A. Alsaed, T. Hayat, and Z. Tan, "Manipulating the trade-off between quantum yield and electrical conductivity for high-brightness quasi-2D perovskite light-emitting diodes," Adv. Funct. Mater. **28**(47), 1804187 (2018).
[52]M. Kim, S. G. Motti, R. Sorrentino, and A. Petrozza, "Enhanced solar cell stability by hygroscopic polymer passivation of metal halide perovskite thin film," Energy Environ. Sci. **11**(9), 2609–2619 (2018).

24 December 2023 15:22:00

© Author(s) 2023